



HAL
open science

Measurement of the radicals' kinetics in pulsed plasmas by UV and VUV absorption spectroscopy and by modulated beam mass spectrometry

G. Cunge, P. Bodart, M. Brihoum, F. Boulard, T. Chevolleau, N. Sadeghi

► To cite this version:

G. Cunge, P. Bodart, M. Brihoum, F. Boulard, T. Chevolleau, et al.. Measurement of the radicals' kinetics in pulsed plasmas by UV and VUV absorption spectroscopy and by modulated beam mass spectrometry. *Plasma Sources Science and Technology*, 2012, 21, pp.024006. 10.1088/0963-0252/21/2/024006 . hal-00944915

HAL Id: hal-00944915

<https://hal.science/hal-00944915>

Submitted on 19 Dec 2022

HAL is a multi-disciplinary open access archive for the deposit and dissemination of scientific research documents, whether they are published or not. The documents may come from teaching and research institutions in France or abroad, or from public or private research centers.

L'archive ouverte pluridisciplinaire **HAL**, est destinée au dépôt et à la diffusion de documents scientifiques de niveau recherche, publiés ou non, émanant des établissements d'enseignement et de recherche français ou étrangers, des laboratoires publics ou privés.

Measurement of free radical kinetics in pulsed plasmas by UV and VUV absorption spectroscopy and by modulated beam mass spectrometry

G Cunge, P Bodart, M Brihoum, F Boulard, T Chevolleau and N Sadeghi

Laboratoire des Technologies de la Microélectronique, CNRS, 38054, Grenoble, France

Abstract

This paper reviews recent progress in the development of time-resolved diagnostics to probe high-density pulsed plasma sources. We focus on time-resolved measurements of radicals' densities in the afterglow of pulsed discharges to provide useful information on production and loss mechanisms of free radicals. We show that broad-band absorption spectroscopy in the ultraviolet and vacuum ultraviolet spectral domain and threshold ionization modulated beam mass spectrometry are powerful techniques for the determination of the time variation of the radicals' densities in pulsed plasmas. The combination of these complementary techniques allows detection of most of the reactive species present in industrial etching plasmas, giving insights into the physico-chemistry reactions involving these species. As an example, we discuss briefly the radicals' kinetics in the afterglow of a $\text{SiCl}_4/\text{Cl}_2/\text{Ar}$ discharge.

1. Introduction

As the semiconductor industry continues to scale down the dimensions of IC circuits, current applied plasma etching processes are showing severe limitations [1]. The introduction of new materials in integrated circuits, the necessity to control the dimensions of the etched features on 300 mm diameter wafers at the nanometer scale and the etching of a few nanometers thick layers with quasi-infinite selectivity are among the challenges that push equipment suppliers to introduce new methods of operation of plasma reactors. Pulsed plasmas [2, 3] and new plasma chemistries are new strategies to improve process control and reproducibility. However, our ability to overcome technological issues is limited by the lack of understanding of the elementary mechanisms involved in these discharges. Furthermore, there are so many controls in an etching reactor that the empirical approach used in the past for process development has become very time-consuming and expensive and it has become necessary to understand the basic processes involved in plasma etching.

In many plasma etching processes, the etching anisotropy and the etching selectivity between materials rely on the

selective formation of a deposit (passivation layer) on the features' sidewalls or on the underlying layer, which blocks the etching. These blocking layers are formed from the redeposition of radicals on surfaces and it is thus of primary importance to measure the sticking probability of these species on different surfaces. This allows us to identify the radicals that play an important role in the process. It thus becomes possible to build a strategy for the control of the density of these radicals by means of the reactor controls and thus to improve the process control. In addition, this approach also allows understanding of the formation mechanisms of polymer layers on the reactor walls, which is well known to impact the wafer-to-wafer reproducibility [4–10].

However, while the measurement of the time-averaged radicals' density can be achieved with the usual diagnostic techniques, it is typically much more difficult to deduce their surface loss probability. A particularly powerful approach to determine the radicals' sticking coefficient on surfaces was introduced by Booth *et al* [11, 12] in the late 1980s: the decay rate of the radicals' density, measured in the afterglow of pulsed discharge by laser-induced fluorescence (LIF), can be directly related to the radical sticking coefficient on the chamber walls

using a simple analytical model based on diffusion. For example, the decay rate in the afterglow of a radical X, assumed to be lost only on the reactor walls, is given by [13]

$$[X] = [X]_0 e^{-k_{\text{walls}} t} \quad (1)$$

$$\frac{1}{k_{\text{walls}}} = \frac{p\Lambda^2}{D} + \frac{V}{A} \frac{2(2-\alpha)}{v_{\text{th}}\alpha} \quad (2)$$

where $[X]_0$ is the radical density at time zero, when the rf is switched off, p is the gas pressure in Torr, D is the diffusion coefficient at 1 Torr, Λ is the characteristic diffusion length, $1/\Lambda^2 = (\pi/L)^2 + (2.405/R)^2$ for a cylindrical reactor with L the reactor height and R its radius. v_{th} is the mean thermal speed of the radicals and V/A the volume-to-surface ratio of the reactor.

We emphasize that the strength of this technique is that only relative density measurements are needed to deduce the decay rate of the density, from which the sticking coefficient is extracted. However, this technique can only provide a ‘chamber surface averaged’ sticking coefficient. Furthermore, equation (2) implicitly assumes that the plasma radicals are lost only by sticking on the reactor walls, neglecting the possibility of chemical reactions in the gas phase. This assumption is often valid in low-pressure discharges but not always, as discussed below. Finally, recent works [14–17] have shown that care must be taken when analyzing the first millisecond of the afterglow period, during which the gas temperature cools down (leading to convection phenomena) which can lead to a non-exponential decay of the radicals’ densities at the measurement point. Nevertheless, this technique remains simple and powerful if one takes account of the above-mentioned limitations. However, until recently, the only diagnostic that was sensitive enough to probe the time evolution of small polyatomic radicals’ density in the afterglow of a low-pressure discharge was the sophisticated and expensive LIF diagnostic technique. As a result, only a few experimental results in fluorocarbon plasmas have been reported using this technique [12, 14, 15, 18–21].

We have recently shown [22] that broad-band absorption spectroscopy, which is much less expensive, can be used for these measurements [23, 24]. This has been possible, thanks to the introduction of the light-emitting diode (LED) as a broad-band light source [25]. The stability of the LED emission intensity allows signal accumulation during many plasma pulsing periods and time-resolved measurements, synchronized with the plasma pulses, can be used to monitor the radical kinetics in the afterglow of pulsed discharges. In this paper, we will first review ultraviolet absorption spectroscopy (UVAS) with LEDs and we will then show that this technique can be extended [26] to the vacuum ultraviolet (VUV) spectral range (125–200 nm), which allows us to detect many species which do not absorb light in the UV-visible range accessible to the LEDs. Finally, we have also developed a specific set-up to measure the time variation of the radical density in pulsed discharges by modulated beam threshold ionization mass spectrometry (MS) [27, 28]. Although more complex, this technique gives access to radicals (in particular atomic species) that could not be detected by

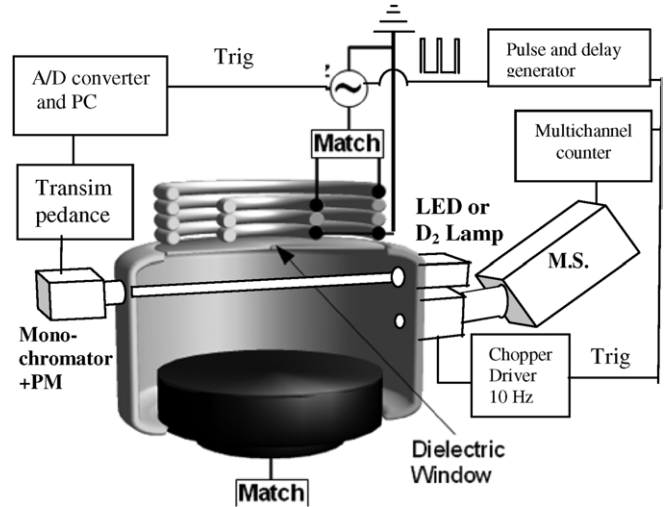


Figure 1. Schematics of the plasma reactor and diagnostics.

optical absorption. As a result, by combining these three techniques, it is possible to analyze the loss and production kinetics of all the plasma radicals present in complex plasma etching chemistries. As an example, we will briefly discuss the physico-chemistry of $\text{SiCl}_4/\text{Cl}_2$ plasmas.

2. Experimental set-up and plasma diagnostics

2.1. Plasma reactor

The experimental set-up has been extensively described elsewhere [2, 22, 29]. Briefly, we are using a commercial DPS reactor from Applied Material designed to etch 300 mm diameter wafers. The reactor has 50 cm diameter and 17 cm height, with both the reactor body and roof made of Al_2O_3 . The reactor body is maintained at 65 °C. As shown in figure 1, the plasma is excited with a dual RF coil which allows improvement of the ion flux uniformity (the current ratio between inner and outer coils is driven by a variable capacitor). The vertical wrapping of the coils allows reduction of the capacitive coupling between the coil and the plasma thus minimizing the sputtering of the reactor roof by energetic ions. As shown in figure 1, the optical ports used for absorption spectroscopy are located 5 cm below the roof of the reactor, and we are thus probing the radicals’ density in the densest region of the plasma. In contrast, MS measurements are carried out near the reactor walls, 13 cm below the reactor roof, as shown in figure 1.

2.2. Time-resolved radical density measurement with broad-band ultraviolet absorption spectroscopy with UV LEDs

Small polyatomic radicals play a major role in etching plasmas and it is important to measure their densities. Among other diagnostics, UV-visible absorption spectroscopy [23, 24, 30] has several advantages: it is a relatively cheap, simple and quantitative technique. In broad-band ultraviolet absorption spectroscopy (BBUVAS), a light beam of intensity $I_0(\lambda)$

is passed through the plasma, and the spectrally resolved attenuation of the beam intensity (due to the absorption of photons by the plasma radicals) is measured by a monochromator backed with a photodiode array or with a photomultiplier tube (PMT), as shown in figure 1. The beam attenuation is evaluated by measuring the intensity of the transmitted light beams, $I_T(\lambda)$ with the plasma on and $I_0(\lambda)$ with the plasma off and the ratio $I_T(\lambda)/I_0(\lambda)$ provides the absorption spectrum. The line-of-sight averaged radical density N is then deduced from the absorption spectrum according to the Beer–Lambert law:

$$\frac{I_T(\lambda)}{I_0(\lambda)} = \exp(-A(\lambda)) \quad (3)$$

where $A(\lambda) = NL\sigma(\lambda)$ is the absorbance, L the plasma size and $\sigma(\lambda)$ the wavelength-dependent absorption cross section.

However, the acquisition of the absorption spectrum is not straightforward since four different measurements with the lamp and plasma on and off must be carried out to subtract the plasma emission and the background noise [23, 31]: $I_T/I_0 = (L_p - P)/(L - B)$, where L_p is the measured intensity with both the lamp and plasma on, P with only the plasma on, L with only the lamp on and B with both the lamp and plasma off. The main issue associated with this technique is that a minimum time interval (up to 30 s) is necessary between L_p , L and P measurements. Consequently, any variation in the lamp intensity spectral distribution or in the plasma emission intensity between the measurements may lead to significant errors in the absorption spectrum. The commonly used Xe or D₂ arc lamp sources for absorption experiments are unstable and lead to the distortion of the baseline of the absorption spectra [31], which reduces considerably the sensitivity of the technique (only absorbances well above the fluctuations of the unabsorbed baseline can be readily measured). Furthermore, to measure the absorbance as a function of time in pulsed discharges, it is necessary to synchronize the acquisition system with the plasma pulses and to accumulate the signal over many plasma pulses: this is possible only if $I_0(\lambda)$ is perfectly stable. This is why we have recently proposed [25] to replace in BBUVAS experiments the Xe or D₂ lamp by a UV LED. We have shown that the LED emission spectrum stability is about 10^{-4} on timescales of a few minutes provided that the LED is thermo-regulated and fed with a stabilized current source. Thanks to the high stability of the LED emission spectrum I_0 , time-resolved measurement of the radicals densities *in pulsed discharges* (with a few μ s time resolution) can be carried out using LEDs in BBUVAS [22]. For these measurements, the monochromator wavelength is fixed on an absorption band, and we use a PMT to measure the transmitted intensity, as shown in figure 2. The output of the PMT is amplified by a transimpedance amplifier, having 10^5 V A^{-1} gain and 100 kHz band-pass, and recorded by a 16 bit analog/digital converter (A/D) triggered by the plasma pulse generator. As shown in figure 2, by averaging over 2000 plasma periods (a 60 s long experiment), an absorbance of 5×10^{-4} can be measured with this system with a signal-to-noise ratio of about 10.

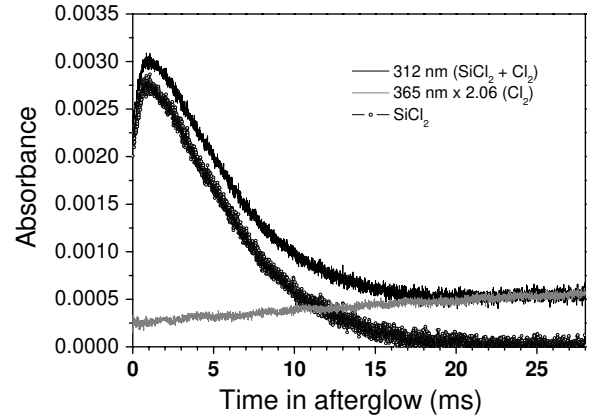


Figure 2. Time variation of the absorbance measured at 312 nm (which includes contributions from Cl₂ and SiCl₂) and at 365 nm (Cl₂ alone). The absorbance at 365 nm has been multiplied by 2.06 to account for the difference in the Cl₂ absorption cross sections at 365 and 312 nm. The time variation of the SiCl₂ density (dotted curve) has been obtained by subtracting the Cl₂ contribution from the absorbance at 312 nm. Plasma conditions: Ar (100 sccm)/Cl₂ (100 sccm)/SiCl₄ (60 sccm) at 10 mTorr with 800 W RF power pulsed at 30 Hz with 15 % duty cycle.

Although quite rare, a potential difficulty associated with this technique is an accidental overlap of absorption spectra of different species. For example, the absorbance measured at 312 nm is mostly due to the SiCl₂ radicals but also contains a small contribution from Cl₂ at this wavelength [24]. To remove that problem, the Cl₂ absorbance is also measured at 365 nm, where it is the only absorbing species and the time variation of the Cl₂ contribution at 312 nm can then be subtracted from the measured signal to obtain the time variation of the SiCl₂ density alone, as shown in figure 2. The 2.06 factor, by which the measured absorbance of Cl₂ at 365 nm is multiplied, accounts for the measured difference in absorption cross-sections of Cl₂ at 312 and 365 nm. This coefficient is close to the 1.9 given by Gibson *et al* [32].

In the following, Cl₂ molecules are detected at 362 nm using a 365 nm LED (Nishia), SiCl is detected at 287 nm with a 285 nm LED (UVTOP) and SiCl₂ is detected at 312 nm with a 315 nm LED (UVTOP). The absorption cross sections of SiCl and SiCl₂ at these wavelengths are given by Kogelschatz *et al* [24] and that of Cl₂ by Gibson *et al* [32].

2.3. Time-resolved radical density measurement with broad-band VUV absorption with a D₂ lamp light source

BBUVAS is a powerful technique but it gives access to only a restricted number of reactive species. In particular, closed shell molecules and atomic species typically do not absorb light in the UV–visible spectral range. For instance, the detection of larger, closed shell molecules is impossible and relies on the use of more sophisticated laser absorption techniques in the infrared region [33–36] or by MS [28, 37]. However, many of these molecules have Rydberg states or pre-dissociated continua which absorb in the VUV spectral range. In etching plasmas, examples of relevant molecules that could be detected in the VUV region include Cl₂, HBr, BrCl, Br₂, HCl, BCl₃, SiCl₄, SiF₄, CCl₄, SF₆, CH₂F₂ and O₂. Most of these

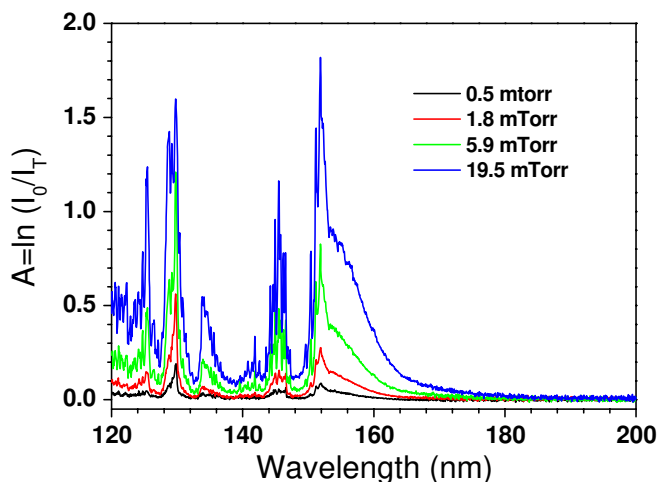


Figure 3. VUV absorption spectrum of Cl_2 gas at different pressures without plasma.

molecules have no transitions accessible in the UV–visible domain, or the transition probability is not large enough for providing measurable absorption rate in low-pressure plasmas. Since the electronic transitions from the ground state to the Rydberg states of molecules often have very large probabilities, VUV absorption spectroscopy is promising for the detection of those molecules with a high sensitivity and it should be complementary to typical UV–visible absorption spectroscopy. Our recent results have shown that this is the case [26]. Furthermore, the absorbance on transitions to Rydberg states being very strong, the issue of the lamp stability associated with absorption experiments in the UV visible range is much less important and time-resolved measurements can be achieved using a D_2 lamp. The main difference between UV and VUV AS is that the totality of the optical path (including the monochromator) must be under vacuum. The experimental set-up has been described in detail in [26].

Figure 3 shows the VUV absorption spectrum of Cl_2 gas at various pressures (without plasma). The absorption rate at 151 nm reaches 85% for a Cl_2 pressure of 20 mTorr. It can also be seen in this figure that the absorbance of the transitions to Rydberg states is strongly saturated (on sharp peaks, $A(\lambda)$ does not vary linearly with pressure). This is because each of the observed peaks is in reality composed of many rotational lines, having a Doppler width of about 0.00025 nm, and of non-absorbing regions between these lines. As the spectral width of these lines is much smaller than the 0.2 nm spectral resolution of the monochromator we are using, we can conclude that with the measured absorbance in the range of unity, the absorption on the positions of rotational lines is almost total (for more details see [38]). Hence, for transitions to the Rydberg states, the medium cannot be considered as optically thin, even at low Cl_2 density. Fortunately, this non-linearity is not an issue since most of the molecules accessible in the VUV are stable (i.e. available as commercial gases): it is thus possible to experimentally determine the relation between the measured I_T/I_0 and the density and to calibrate the Cl_2 density on an absolute scale. Furthermore, in addition to the Rydberg states, many molecules have also weak transitions

toward predissociated states which show up as non-saturated continuums. For Cl_2 , such a continuum is observed between 155 and 190 nm. If a good enough S/N ratio can be achieved, it is advantageous to use the continuum part of the spectrum to analyze the time variation of the density in pulsed plasmas since the data can be directly used without the need for applying a non-linear correction to the measured data.

2.4. Time-resolved radical density measurement by modulated beam threshold ionization MS

MS has proven to be an effective plasma diagnostic tool. This is mainly due to the MS ability to sample *in situ* stable atoms, molecules, radicals and positive or negative ions. Time-resolved measurements of radicals' densities in pulsed discharges by MS have been reported but remain complicated [13, 39]. First, in MS, the radicals must be ionized in the MS head by an electron beam. In the case of radicals/atoms, threshold ionization must be used to separate the ions originating from the direct ionization of the radical from the signal originating from the dissociative ionization of larger molecules [27, 40, 41]. This is not an issue, but working near threshold implies a low signal level, which is not favorable for time-resolved measurements. Furthermore, accurate MS measurements require subtraction of the so-called background signal [28, 40, 42]. Indeed, a typical MS signal contains two components: from the beam and the background. The beam signal corresponds to radicals that have been directly ionized immediately after having crossed the sampling orifice on the reactor wall and entering the MS ionization volume, while the background signal corresponds to radicals that have bounced several times on the surfaces inside the MS head before being ionized. In other words, the background signal originates from the residual partial pressure of the radicals in the MS head. Since only the beam signal is proportional to the radicals' density in the plasma volume, it is necessary to subtract the background signal from the measured data. This can be achieved using modulated beam MS (MBMS), in which a mechanical chopper is used to modulate the beam entering the ionization chamber. When the beam is blocked, only the background signal is measured and it can be subtracted from the total signal measured with the open chopper to get the beam component alone. MBMS requires sophisticated equipment with at least two stages of differential pumping (the mechanical chopper being located in between these stages). Double or triple differential pumping allows reduction of the amplitude of the background signal [28]. In our system, as shown in figure 4, the radicals are sampled from the plasma through an orifice (0.7 mm diameter) and they enter a first vacuum chamber (in which the chopper is located) pumped by a turbomolecular pump. They can then pass through a second orifice (1.5 mm diameter) to enter the MS ionizer chamber which is differentially pumped by another turbomolecular pump. The vacuum in this system is about 10^{-7} Torr in the MS head and 10^{-6} Torr in the first chamber, when the reactor is operating at 10 mTorr and one order of magnitude smaller when the reactor is empty. Furthermore, since the radical beam that is passing through the first hole is diverging, it

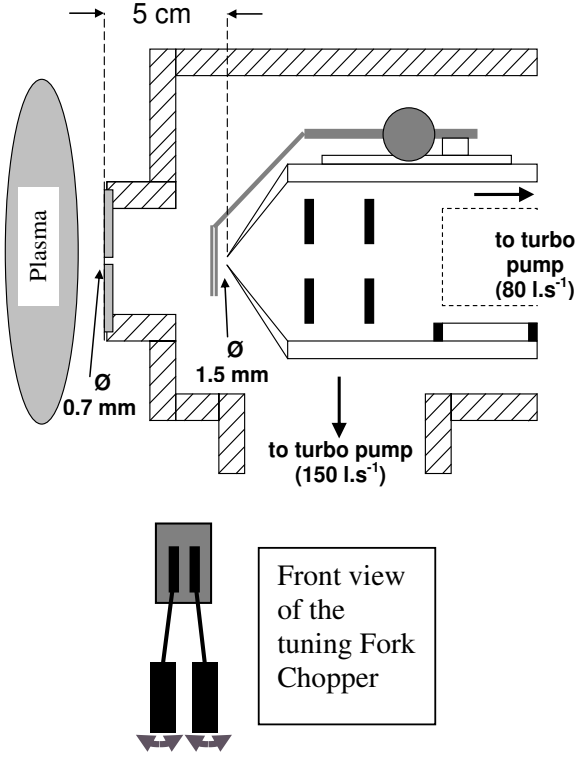


Figure 4. Schematic of the mass spectrometer head (modified hidden EQP 500) with the tuning fork chopper fitted on the top of the MS ionization chamber.

is important to minimize the distance between the holes to enhance the beam-to-background ratio (the beam signal drops roughly as the square of this distance). This requires the use of a specific chopper design. We used a electromechanically driven tuning fork resonant chopper (figure 4), which works at fixed frequency. Vanes attached to the moving tines of the fork modulate the beam that is passing through the blades. The chopper operates at the natural resonant frequency established by the effective mass of the moving assembly and the spring constant of the tines (10 Hz in our system). The choice of this chopper allowed us to reduce the distance between the two holes down to about 1 cm. However, this distance was eventually increased to 5 cm to allow the sampling hole to be located at the inner wall position of the reactor (as shown in figure 4) and not behind the plasma/wall boundary.

It is important to emphasize that the previous authors [28, 40] who investigated MBMS in reactive plasmas, assumed that the background intensity is independent of the chopper position (i.e. closed or open). However, as discussed below, this assumption is not always valid since a significant part of the background can originate from the beam itself, which causes a small overpressure in the MS head (not all the molecules from the beam are ionized, and some of them remain for a while in the MS head before being pumped out). In our system, with the chopper oscillating at 10 Hz, it is necessary to record the time variation of the MS signal during the chopping period (100 ms). In commercially available systems, this measurement is usually done by a boxcar system, which for a fixed number of the plasma cycles integrates the signal counts during a short time window Δt , opened at time t relative to

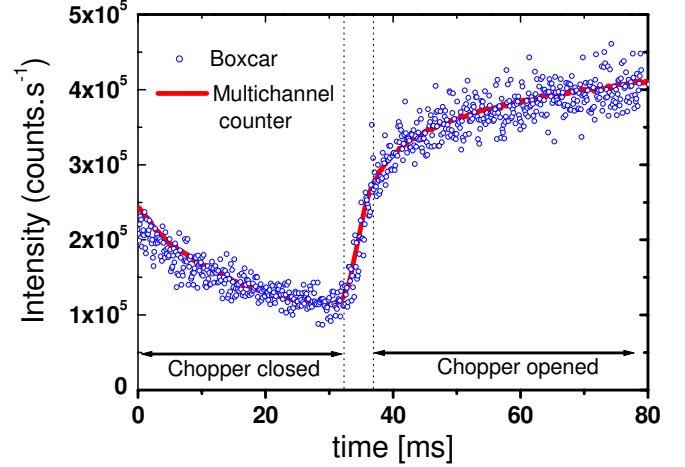


Figure 5. MS signals versus time during the opening of the chopper at $m/e = 40$ in pure Ar gas at 5 mTorr. Open symbols: data with a boxcar, solid line: data for the same acquisition time with a multichannel counter.

the discharge pulse, and stores it in the computer. The boxcar window is then successively shifted to other time-delay and so on, until the entire discharge period is recorded. This procedure is very inefficient since in each plasma period the signal is taken only during the short time window of the boxcar gate. We have thus replaced this system by a multichannel pulse counter [43] (MCS-pci from ORTEC), which captures the signal during the entire chopper period. Basically, the counter works like many boxcars in parallel. It is triggered by a synchronization signal from the chopper (as shown in figure 1) and the pulsing period is divided into channels (typically 1000 in the following). According to the arrival times in the pulsing period of the ion pulse from the channeltron of the MS, the counts are stored in different channels of the counter. To highlight the difference between these two acquisition methods, figure 5 shows the time variation during one chopping period of the signal at $m/e = 40$ (the reactor is filled with 5 mTorr of Ar gas without plasma) recorded either with boxcar or multichannel counter. As seen in this figure, for the same total acquisition time, the S/N is improved by a factor of about 20 when a multichannel counter is used. This means that 400 times longer acquisition time is necessary to get the same S/N with the boxcar than with the multichannel analyzer. This enhancement of the S/N is the key to achieve time-resolved measurements in pulsed discharges that are discussed below. Figure 5 also shows that the background signal of argon is high and that the time variation of the signal during the chopper period exhibits unexpected features: the signal does not rise abruptly when the chopper opens. To get insight into these features, we have analyzed signals from O and O₂ species in pure O₂ continuous plasma. Figure 6 shows the variations of the signal at $m/e = 16$ (O atoms) as a function of the electron energy both with the plasma on and off. When the plasma is off, the O⁺ ions detected by the MS originate from the dissociative ionization of O₂ molecules, while with the plasma ON both direct ionization of O atoms and dissociative ionization of O₂ can produce O⁺ ions. However, since the threshold for dissociative ionization of O₂ is about 19 eV while the threshold

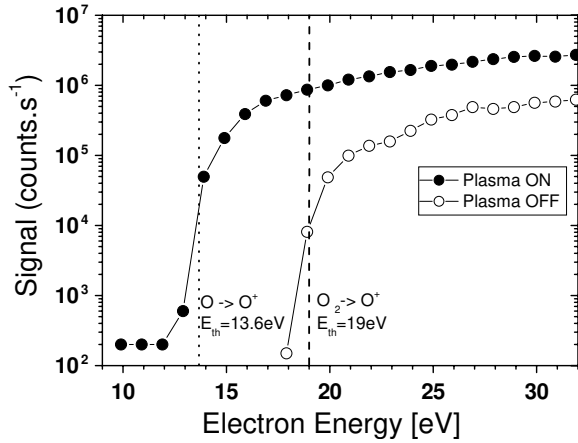


Figure 6. MS signals at $m/e = 16$ (O atoms) versus electron energy with the plasma on and off. Plasma conditions: 10 mtorr O_2 pressure, 800 W RF ICP power.

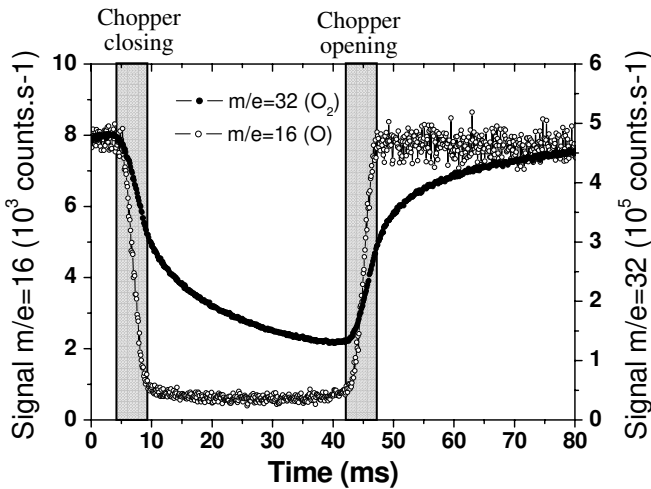


Figure 7. MS signals versus time during the closing and the opening of the chopper at $m/e = 16$ with an electron energy set at 15 eV (O radical) and at $m/e = 32$ at 25 eV. Plasma conditions: 10 mtorr O_2 pressure, 800 W RF ICP power. The shaded area indicates the time windows during which the chopper opens and closes.

energy for direct ionization is only 13.6 eV, there is a rather large electron energy window in which the signal originates only from the direct ionization of O atoms. In the following, we have chosen an electron energy of 15 eV to monitor either O atoms at $m/e = 16$ and O_2 molecules at $m/e = 32$ present in the plasma.

Figure 7 shows the time variation of the signals at mass 16 and 32 (O and O_2) during one chopping period. The measurement is carried out in a pure O_2 plasma at a pressure of 10 mTorr and 800 W RF power. There is a remarkable difference between the O and O_2 behaviors. The signal from O atoms drops sharply when the chopper closes, as expected. From figure 7 we deduce that it takes about 5 ms for the blades to fully shut down the beam. During the fully closed period of the chopper (10–40 ms in figure 7), we measure the background signal, which is very small in this case. Then the chopper opens and the O atom signal rises rapidly and for $t > 50$ ms the recorded signal corresponds to the beam+background. By

contrast, the signal of O_2 molecules at $m/e = 32$ continues to decay even after the shut down of the beam (and it continues to rise after the full opening of the chopper), as was the case for Ar atoms in figure 5. This unexpected behavior is observed because a large part of the O_2 background originates from the beam: after the total shut down of the beam at $t = 10$ ms, it takes some time to pump out the O_2 molecules that entered the MS head when the chopper was open. Therefore, the background signal at $m/e = 32$ decays exponentially with a time constant corresponding to the residence time of O_2 molecules in the MS head. This result shows that to prevent an underestimation of the background level, it is crucial to measure the background signal intensity just after the beam has been shut down. Another interesting feature in figure 7 is that the beam-to-background level depends strongly on the chemical reactivity of the species: the background at $m/e = 16$ is small because O atoms are so reactive that their partial pressure in the MS head remains negligibly low (they are ‘pumped’ at a very high rate by the MS surfaces on which they stick with high probability). In contrast, O_2 molecules have a near-zero surface reaction probability and are lost from the MS head only by the pumping system, leading to a high background level that is varying with time.

Finally, time-resolved measurements in a pulsed discharge require a proper synchronization between the chopper, the plasma pulses and the trigger signal of the multichannel analyzer. As shown in figure 1, this synchronization is achieved using the 10 Hz modulation signal from the chopper to trigger both the acquisition system and the plasma pulses. More precisely, a burst/delay function generator produces bursts of N pulses at each trigger signal from the chopper. These pulses, at a frequency of $N \times 10$ Hz, are then used to pulse the plasma power supply. The number of pulses in each chopper cycle and their length are controllable and allow adjustment of the plasma pulsing frequency and duty cycle. Figure 8 shows an example in which the signal generator produces bursts of $N = 3$ pulses per trigger, i.e. the plasma pulsed at 30 Hz. The upper part of the figure indicates schematically the synchronization sequences, while the lower part shows the signal of Cl atoms recorded at $m/e = 35$ with an electron energy of 15 eV (below the threshold energy of 15.7 eV for the dissociative ionization of Cl_2) in a $SiCl_4/Cl_2/Ar$ plasma. The important point in this measurement is to adjust the plasma pulsing frequency and the delay between the chopper opening and the plasma pulses so as to get a full plasma period during the time when the chopper is fully open. The result shown in figure 8 was averaged over 300 chopping periods (30 s). The signal is then treated as follows: the background measured between times 0 and 15 ms is subtracted and then the signal during one plasma pulse is isolated ($35 < t < 70$ ms). Finally, to convert this signal of counts/s into an absolute density, the reactor is filled with 10 mTorr of Ar gas and the signal at $m/e = 40$ is recorded with 25 eV ionization electron energy. This relation between c/s and density in Ar is then transferred to the Cl atoms’ density, by accounting for the differences in ionization cross sections of the species [27]. Since Ar and Cl have comparable masses, we assume an identical transport efficiency of these ions within

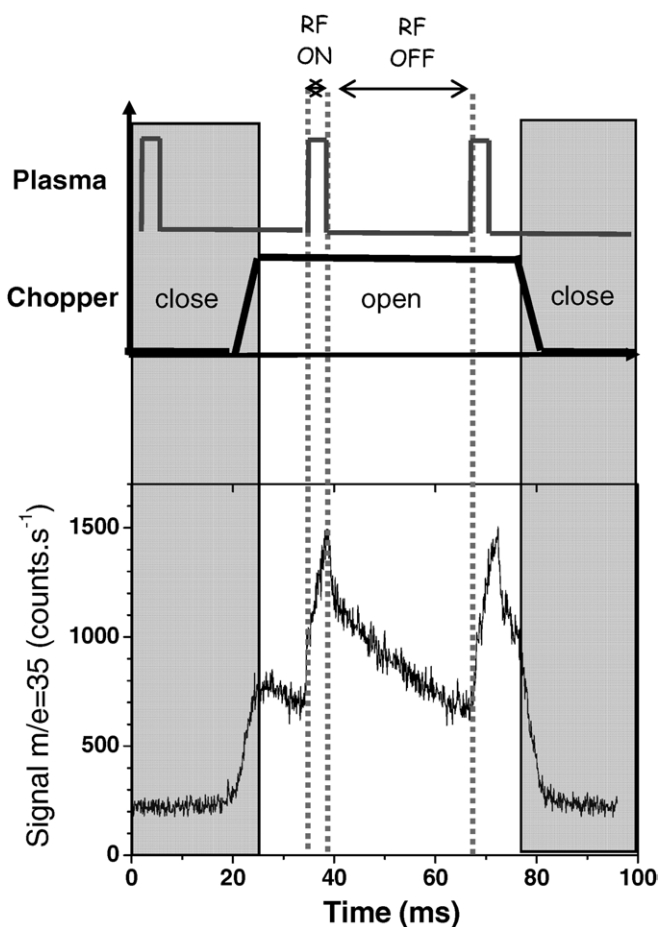


Figure 8. Upper part: timing of the chopper and plasma pulses for time-resolved measurement by MS. The chopper is oscillating at 10 Hz and this signal is used to produce bursts at 30 Hz that, in turn, are used to generate the plasma pulses. The chopper also triggers the multichannel analyzer acquisition (lower part). In the example, Cl atoms at $m/e = 35$ are detected from a $\text{SiCl}_4/\text{Cl}_2/\text{Ar}$ pulsed plasma: Ar (100 sccm)/ Cl_2 (50 sccm)/ SiCl_4 (60 sccm) at 10 mTorr with 800 W RF power pulsed at 30 Hz with 15% duty cycle

the MS. The uncertainty on the absolute density calibration is estimated to be better than 30%.

3. Result and discussion: radicals' kinetics in $\text{SiCl}_4/\text{Cl}_2/\text{Ar}$ plasmas

$\text{SiCl}_4/\text{Cl}_2$ based mixtures are interesting for several applications in field of plasma etching processes [44–46]. However, little information is available on the radicals' kinetics in such plasmas. Actually, the interaction of SiCl_x radicals with surfaces has been studied in the frame of silicon etching by Cl_2 plasmas (in which SiCl_4 is the by-product of the wafer etching) [9, 16, 37, 47–50].

Figure 9 shows the time variations of the SiCl_x ($x = 1-4$) and Cl_x ($x = 1-2$) densities in the afterglow of a SiCl_4 (60 sccm)/ Cl_2 (50 sccm)/Ar (100 sccm) plasma at 10 mTorr and excited by 800 W RF power pulsed at 30 Hz with 15% duty cycle. Only the afterglow period is considered in this paper. SiCl and SiCl_2 are measured by UVAS, SiCl_4 and Cl_2 by VUVAS and SiCl_3 and Cl by MBMS. In the discussion

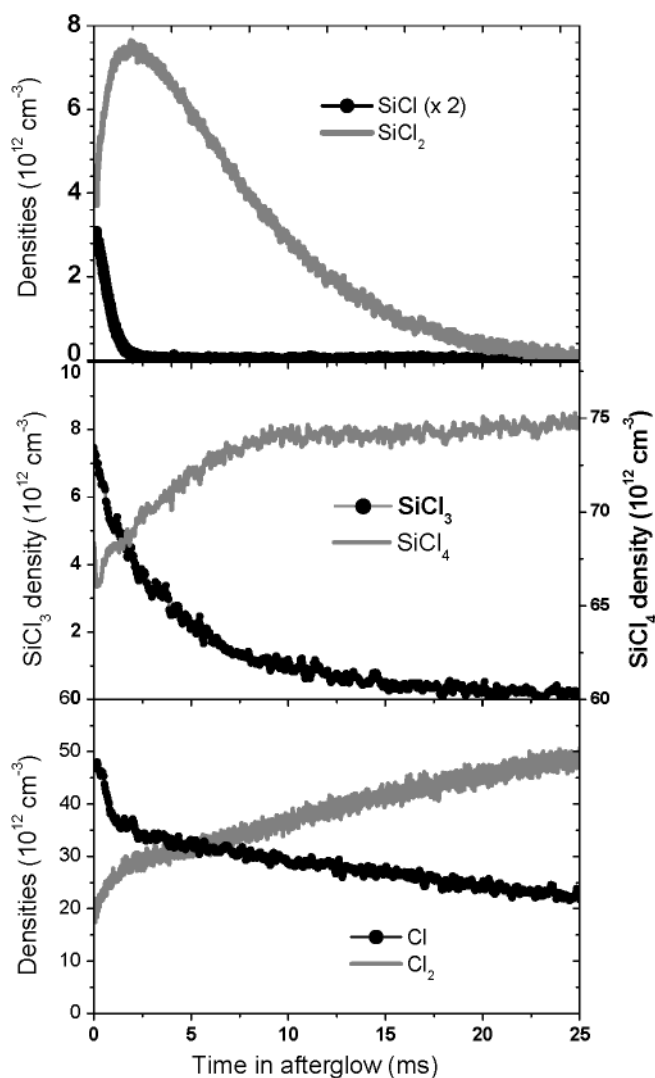
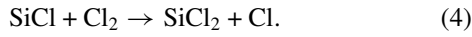


Figure 9. Time variation of the radicals' densities in the afterglow of a pulsed plasma. Plasma conditions: Ar (100 sccm)/ Cl_2 (50 sccm)/ SiCl_4 (60 sccm) at 10 mTorr with 800 W RF power pulsed at 30 Hz with 15% duty cycle. Upper graph: SiCl and SiCl_2 densities (measured by UVAS). Middle graph: SiCl_3 and SiCl_4 measured by MS and VUVAS, respectively. Lower graph: Cl and Cl_2 measured by MS and VUVAS, respectively.

below, we will not try to compare quantitatively the densities measured by MS with those obtained by optical diagnostics since the measurements are carried out at two different locations in the reactor (figure 1). However, figure 9 shows that by combining different diagnostic techniques, we are able to study the time evolution of all relevant species present in this complex chemistry. Nevertheless, the interpretation of these data remains a challenge. This is for a large part due to the fact that some of these radicals are lost/produced by chemical reactions both on the reactor wall surfaces and in the gas phase. The importance of gas phase reactions in low-pressure plasmas has been often underestimated in the past. However, exchange reactions can proceed at high rates, with weak dependence on the total pressure. For example, our recent work has shown that such reactions are important in BCl_3/Cl_2 plasmas [22] and $\text{SiCl}_4/\text{Cl}_2$ discharges [16]. In the latter case, reaction (4)

proceeds at a rate approaching the collision frequency:



The fingerprint of this fast reaction is clearly visible in figure 9: in the afterglow, the SiCl density drops rapidly while the SiCl₂ density increases due to its production by this reaction. It is interesting to point out that because of this reaction SiCl is lost at a rate $k = 1750 \text{ s}^{-1}$, which is far above its maximum possible loss rate on the surface (480 s^{-1} according to equation (2)). Therefore, if we neglect pumping, the loss rate of SiCl in the afterglow is the sum of two contributions:

$$k_{\text{loss}} = k_{\text{wall}} + k_{\text{gas}}[\text{Cl}_2] \quad (5)$$

where k_{wall} is the SiCl loss rate on the reactor walls (linked to its loss probability by equation (2)) and k_{gas} is its reaction rate with Cl₂ molecules. To separate these two contributions, it is necessary to measure the SiCl loss rate for various dilutions of Cl₂ in order to plot k_{loss} as a function of the Cl₂ density: the resultant line has a slope k_{gas} and an origin at zero Cl₂ equal to k_{wall} . From this analysis, we conclude that SiCl is lost on the reactor walls with a probability of about 100%. We emphasize that a large part of this surface loss is due to the abstraction of Cl from the surface (forming SiCl₂ which returns in the plasma) and not due to simple sticking.

Figure 9 also shows that after its initial increase, the SiCl₂ density decays slowly in the afterglow. This decay rate (145 s^{-1}) is low enough to be attributed solely to the surface reactions. However, complementary experiments (to be published) with various dilutions of Cl₂ indicate that the SiCl₂ loss rate increases with the Cl₂ density. It is thus difficult to ascertain if SiCl₂ is solely lost on the reactor walls or also by a reaction analogous to equation (4). However, if SiCl₂ had to react with Cl₂ to form SiCl₃, we would expect to see a significant production of SiCl₃ in the afterglow. This is not observed in figure 9, which shows that the shapes of the time evolution of SiCl₂ and SiCl₃ are not correlated. Therefore, we conclude that SiCl₂ is lost on the reactor walls where it probably reacts with Cl₂ to produce SiCl₄. With this hypothesis, the SiCl₂ loss rate will depend on the amount of Cl₂ resident on the surfaces and thus on the Cl₂ density in the plasma.

By contrast, figure 9 suggests that SiCl₃ is converted into SiCl₄ since the decay rate of the SiCl₃ density corresponds well to the rise rate of the SiCl₄ density. Again, this can be attributed to a reaction between SiCl₃ and chlorine either in the plasma or at the surfaces. However, the gas phase reaction between SiCl₃ and Cl₂ is expected to produce significant amounts of Cl atoms that are not detected by the MS. It is thus expected that SiCl₃ is lost mainly on the reactor walls where it abstracts Cl (either from Cl or Cl₂ resident on the surface) to produce SiCl₄. Therefore, in SiCl₄/Cl₂ plasmas, both gas phase and surface reactions of SiCl_x radicals with chlorine tend to produce more chlorinated radicals, eventually reforming SiCl₄, and SiCl appears to be much more reactive than SiCl₂ and SiCl₃. This explains why the dissociation fraction of SiCl₄ at the end of the on period is only about 10%.

Finally, figure 9 shows another interesting feature: in the early afterglow, there is a sharp rise of the Cl₂ density

accompanied by a sharp drop of the Cl density. After this initial transient time, the Cl atoms' density decays very slowly while the Cl₂ density rises slowly. Indeed the decay rate of Cl corresponds to its pumping rate (1/residence time) while the Cl₂ rise rate is due to the Cl₂ injection in the reactor at a flow rate of 50 sccm. Therefore, figure 9 suggests that in the early afterglow Cl atoms recombine into Cl₂ on the reactor walls at a high rate and that suddenly the surface changes and becomes inert to Cl atoms, which are then only lost by pumping. This is different from experiments in pure Cl₂ without SiCl₄, in which Cl atoms recombine into Cl₂ during the entire afterglow [16]. Furthermore, figure 9 suggests that there is a direct correlation between the presence of SiCl radicals and this surface modification: it seems that the production of Cl₂ occurs only in the presence of SiCl since the initial rise time of the Cl₂ density is always correlated with the decay time of the SiCl density. However, since the variation of the species densities in the first millisecond of the afterglow can also be affected by convection phenomena [17] in the reactor, more experiments and numerical modeling are in course to clarify these surprising phenomena.

4. Conclusion

A variety of plasma diagnostics have been developed to monitor the variation of radicals' densities in the afterglow of pulsed discharges. BBUVAS with LED as a light source is a simple, low cost and powerful technique to detect small polyatomic radicals, and thanks to the stability of the LED emission intensity, time-resolved measurements can be carried out. The extension of the BBAS in the VUV domain allows the detection of more species and in particular closed shell molecules. Transitions toward Rydberg states are very strong and permit time-resolved measurements even with a weakly stable D₂ lamp. Finally, modulated beam threshold ionization MS can be used to detect radicals and atomic species that are not accessible by optical diagnostics. A proper design of the MS spectrometer and acquisition system is required to subtract properly the background signal and to carry out time-resolved measurement. The combination of these three diagnostics allowed us to detect all the neutral species in SiCl₄/Cl₂ based plasmas providing considerable insight into the radical production and loss kinetics in the gas phase and on the reactor wall surfaces.

References

- [1] Lill T and Joubert O 2008 *Science* **319** 1050
- [2] Petit-Etienne C, Darnon M, Vallier L, Pargon E, Cunge G, Boulard F, Joubert O, Banna S and Lill T 2010 *J. Vac. Sci. Technol. B* **28** 926
- [3] Agarwal A, Stout P, Banna S, Rauf S and Collins J 2011 *J. Vac. Sci. Technol. A* **29** 11017
- [4] Ullal S J, Godfrey A R, Edelberg E A, Braly L B, Vahedi V and Aydil E S 2002 *J. Vac. Sci. Technol. A* **20** 43
- [5] Ullal S J, Singh H, Daugherty J, Vahedi V and Aydil E S 2002 *J. Vac. Sci. Technol. A* **20** 1195
- [6] Cunge G, Joubert O and Sadeghi N 2003 *J. Appl. Phys.* **94** 6285

- [7] Cunge G, Kogelschatz M and Sadeghi N 2004 *Plasma Sources Sci. Technol.* **13** 522
- [8] Cunge G, Pelissier B, Joubert O, Ramos R and Maurice C 2005 *Plasma Sources Sci. Technol.* **14** 599
- [9] Cunge G, Sadeghi N and Ramos R 2007 *J. Appl. Phys.* **102** 093305
- [10] Ramos R, Cunge G, Joubert O, Sadeghi N, Mori M and Vallier L 2007 *Thin Solid Films* **512** 4846
- [11] Booth J P, Hancock G, Perry A J, Blaikely D C W, Cairns J A and Smailes R 1987 *Mater. Res. Soc. Symp. Proc* **98** 135
- [12] Booth J P, Hancock G, Perry N D and Toogood M J 1989 *J. Appl. Phys.* **66** 5251
- [13] Perrin J, Shiratani M, Kae-Nune P, Videlot H, Jolly J and Guillon J 1998 *J. Vac. Sci. Technol. A* **16** 278
- [14] Abada H, Chabert P, Booth J P and Robiche J 2002 *J. Appl. Phys.* **92** 4223
- [15] Booth J P, Abada H, Chabert P and Graves D B 2005 *Plasma Sources Sci. Technol.* **14** 273
- [16] Cunge G, Vempeire D, Ramos R, Touzeau M, Joubert O, Bodart P and Sadeghi N 2010 *Plasma Sources Sci. Technol.* **19** 34017
- [17] Cunge G, Vempeire D and Sadeghi N 2010 *Appl. Phys. Lett.* **96** 131501
- [18] Booth J P, Cunge G, Chabert P and Sadeghi N 1999 *J. Appl. Phys.* **85** 3097
- [19] Cunge G and Booth J P 1999 *J. Appl. Phys.* **85** 3952
- [20] Cunge G, Chabert P and Booth J P 1997 *Plasma Sources Sci. Technol.* **6** 349
- [21] Cunge G, Chabert P and Booth J P 2001 *J. Appl. Phys.* **89** 7750
- [22] Vempeire D and Cunge G 2009 *Appl. Phys. Lett.* **94** 21504
- [23] Booth J P, Cunge G, Neuilly F and Sadeghi N 1998 *Plasma Sources Sci. Technol.* **7** 423
- [24] Kogelschatz M, Cunge G and Sadeghi N 2004 *J. Phys. D: Appl. Phys.* **37** 1954
- [25] Cunge G, Vempeire D, Touzeau M and Sadeghi N 2007 *Appl. Phys. Lett.* **91** 231503
- [26] Cunge G, Fouchier M, Brihoum M, Bodart P, Touzeau M and Sadeghi N 2010 *J. Phys. D: Appl. Phys.* **44** 122001
- [27] Singh H, Coburn J W and Graves D B 2000 *J. Vac. Sci. Technol. A* **18** 299
- [28] Singh H, Coburn J W and Graves D B 2000 *J. Vac. Sci. Technol. A* **17** 2447
- [29] Banna S *et al* 2009 *IEEE Trans. Plasma Sci.* **37** 1730
- [30] Childs M A, Menningen K L, Chevako P, Spellmeyer N W, Anderson L W and Lawler J E 1992 *Phys. Lett. A* **171** 87
- [31] Neuilly F, Booth J P and Vallier L 2002 *J. Vac. Sci. Technol. A* **20** 225
- [32] Gibson G E, Rice O K and Bayliss N S 1933 *Phys. Rev.* **44** 193
- [33] Chou S, Baer D and Hanson K 2000 *J. Vac. Sci. Technol. A* **19** 477
- [34] Kim S, Klimecky P, Jeffries J B, Terry F L and Hanson R K 2003 *Meas. Sci. Technol.* **14** 1662
- [35] Röpcke J, Mechold L, Käning M, Fan W Y and Davies P B 1999 *Plasma Chem. Plasma Process.* **19** 395
- [36] Hempel F, Artyushenko V, Weichbrodt F and Röpcke J 2009 *J. Phys.: Conf. Ser.* **157** 012003
- [37] Kogelschatz M, Cunge G and Sadeghi N 2004 *J. Vac. Sci. Technol. A* **22** 624
- [38] Ramos R, Cunge G, Touzeau M and Sadeghi N 2008 *J. Phys D: Appl. Phys.* **41** 115205
- [39] Tserepi A, Schwarzenbach W, Derouard J and Sadeghi N 1997 *J. Vac. Sci. Technol. A* **15** 3120
- [40] Agarwal A, Quax G W W, Van de Sanden M C M, Maroudas D and Aydil E S 2003 *J. Vac. Sci. Technol. A* **22** 71
- [41] Schwarzenbach W, Tserepi A, Derouard J and Sadeghi N 1997 *Japan. J. Appl. Phys* **36** 4644
- [42] Benedikt J, Ellerweg D and Von Keudell A 2009 *Rev. Sci. Instrum.* **80** 055107
- [43] Pelissier B and Sadeghi N 1996 *Rev. Sci. Instrum.* **67** 3405
- [44] Ramos R, Cunge G, Pelissier B and Joubert O 2007 *Plasma Sources Sci. Technol.* **16** 711
- [45] Golka S, Arens M, Reetz M, Kwapien T, Bouchoule S and Patriarche G 2009 *J. Vac. Sci. Technol. B* **27** 2270
- [46] Stern M B and Liao P F 1983 *J. Vac. Sci. Technol. B* **1** 1053
- [47] Cunge G, Kogelschatz M and Sadeghi N 2004 *J. Appl. Phys.* **96** 4578
- [48] Kogelschatz M, Cunge G, Joubert O, Vallier L and Sadeghi N 2004 *Contrib. Plasma Phys.* **44** 425
- [49] Tinck S, Boullart W and Bogaerts A 2011 *Plasma Sources Sci. Technol.* **20** 045012
- [50] Cunge G, Kogelschatz M, Joubert O and Sadeghi N 2005 *Plasma Sources Sci. Technol.* **14** S42